HHS Public Access

Author manuscript

Ceram Int. Author manuscript; available in PMC 2023 September 12.

Published in final edited form as:

Ceram Int. 2022 June 15; 48(12): 17095–17103. doi:10.1016/j.ceramint.2022.02.265.

Composition, processing, and properties of biphasic zirconia bioceramics: relationship to competing strength and optical properties

Chek Hai Lim,

Sonaj Vardhaman,

Niyati Reddy,

Yu Zhang*

Department of Preventive and Restorative Sciences, School of Dental Medicine, University of Pennsylvania, PA 19104, USA

Abstract

A study is made of relationships between composition, processing, structure and properties of biphasic zirconia bioceramics. The focus is on zirconia compositions with different yttria dopant contents used in modern dental restorations, namely 3 – 5 mol% yttria stabilized zirconia (3YSZ, 4YSZ, and 5YSZ). Crystallographies and densities are surveyed, sintering conditions examined, and microstructures characterized. Strength and optical tests are conducted on each YSZ, and dependencies on sintering temperature, cubic content and grain size analyzed. Strength correlates with the amount of tetragonal zirconia (*t*-ZrO_2) crystals with large lattice distortions (tetragonality). YSZ translucency correlates with content of cubic zirconia (*c*-ZrO_2) and *t*-ZrO_2 with low levels of tetragonality. Consistent with literature reporting, the materials rank in decreasing order 3YSZ, 4YSZ to 5YSZ for strength but increasing order for translucency. However, for a given composition, the data suggest that the strengths of densely sintered 3YSZ and 4YSZ actually increase with translucency, although that of 5YSZ remains undiminished. These trends are in apparent contradiction to prevailing experience, and offer potential future processing routes to optimization of clinical materials.

Keywords

crystal structure; microstructure; tetragonality; density; strength; translucency

1. Introduction

Zirconia (ZrO_2) is ostensibly a simple inorganic compound: one zirconium ion (Zr^{4+}) paired with two oxygen ions (O^{2-}). However, it can exist in several crystallographic forms. At atmospheric pressure pure zirconia exhibits three polymorphs: monoclinic (*m*-ZrO_2, baddeleyite, space group $P2_1/c$) from room temperature to 1170°C [1]; tetragonal (*t*-ZrO_2,

***Corresponding Author:** Yu Zhang, Department of Preventive and Restorative Sciences, School of Dental Medicine, University of Pennsylvania, 240 South 40th Street, Levy Bldg. Rm 109, Philadelphia, PA 19104-6030, USA. Tel.: +1 (215) 573-9212, yz21@upenn.edu.

söhngeite, space group $P4_2/nmc$) between 1170°C and 2370°C [2]; and cubic (c-ZrO_2, fluorite, space group $Fm\bar{3}m$) from 2370°C to melting temperature 2700°C [3]. At high pressure, zirconia can also exist in at least three orthorhombic polymorphs [4], including ortho-I (brookite, space group *Pbca*) [5, 6], ortho-II (cotunnite, space group *Pnma*) [7, 8], and ortho-III (boracite, space group $Pca2_1$) [9]. To achieve these high-temperature and high-pressure phases at ambient conditions, zirconia needs to be stabilized, at least partially, by multivalent metal cations [10], Mg^{2+} [11], Ca^{2+} [12], Y^{3+} [13], Ce^{4+} [14], etc. [15–17]. It is the large variety of stabilizing cations and ensuing crystal structures that contribute to many unique mechanical, optical, chemical, thermal, and dielectric properties of zirconia [18–25]. These properties render this one of the most technologically versatile ceramics. Its applications range from extrusion dies and tool bits [26, 27] to refractories [28], from wear-resistant coatings and films [29] to thermal barrier coatings [30, 31], from fuel cells [32, 33] to oxygen sensors [34], and even to jewelry [35]. Critically, zirconia is emerging as a preeminent bioceramic in dental prostheses and restorations, especially in the context of mechanical durability and optical esthetics [21, 36, 37].

The original dental and other biomedical zirconias were predominantly 3 mol% yttria-stabilized tetragonal zirconia polycrystals (3Y-TZP), or simply 3YSZ. This form of zirconia is attractive for its high strength and moderate toughness [36–38]. More recently, 4YSZ and 5YSZ (4 and 5 mol% yttria-stabilized) zirconias with greater cubic phase have been introduced to restorative and prosthetic dentistry for their higher translucency [21], although the stronger but more opaque 3YSZ is still retained for posterior crowns [39] and frameworks for bridges [40], for masking of dischromic abutment teeth [41], and for dental implants and abutments [21]. Biphasic forms of zirconia exhibit a greater degree of freedom for tailoring mechanical and optical properties [42]. But despite extensive attention from researchers in various fields, systematic studies into effects of composition and processing on crystal structure, microstructure, and mechanical and optical properties of YSZ remain incomplete. Some studies have focused on the effect of sintering temperatures [43–48]. Others have investigated crystal structures and functionalities (optical properties and ion conductivities) of cubic zirconia stabilized with ≥ 8 mol% yttria [22, 49–54]. Processing–properties relationships for compositions between 3YSZ and 8YSZ that represent biphasic tetragonal/cubic zirconias are, however, less explored [55, 56]. The fundamental question as to why 3YSZ is intrinsically stronger than 4YSZ but less translucent, even when these two materials have similar tetragonal and cubic phase contents, remain to be satisfactorily answered. The development of novel zirconias is a continuing area of biomaterials research [21].

The present article examines the vital roles of starting composition and sintering temperature on YSZ crystal structures—their polymorphic transformations and microstructural evolution—and their relation to physical, mechanical and optical properties. We present data on crystal structures and lattice parameters for 3YSZ, 4YSZ, and 5YSZ compositions sintered at various temperatures. Based on experimentally determined phase compositions and a modified rule-of-mixture model, we compute theoretical densities of various YSZ compositions using a previously developed and validated method based on spherical ion packing [57, 58]. Finally, we provide explanations for the dependence of mechanical

(strength) and optical (translucency) properties on YSZ compositions and sintering temperatures from crystallography and phase stability standpoints, and explore the potential for future development of materials that optimize these critical properties.

2. Crystallography of zirconia

2.1 Crystal structure

Cubic and tetragonal phases of YSZ will be given special attention here because of their pertinence to translucency as well as to strength properties in dental applications. Cubic zirconia (*c*-ZrO_2) in Fig. 1a comprises four ZrO_2 units, with lattice parameter a_c. In contrast, tetragonal zirconia (*t*-ZrO_2) in Fig. 1b strictly has a body-centered primitive unit cell consisting of two ZrO_2 units (dashed outline). However, for ready comparison with the cubic phase it is convenient to index the tetragonal unit cell to a face-centered supercell with four ZrO_2 units (solid outline). Whereas the *t*-ZrO_2 supercell shares the c axis with the primitive cell, its a_t axis is at 45° to a_p ($a_t = \sqrt{2}a_p$). The ratio c_t/a_t represents the tetragonality. Arrows in Fig. 1b represent the displacement of oxygen atoms in relation to their counterparts in the undistorted cubic structure.

Figure 2 plots experimental unit cell dimensions and volumes for both tetragonal and cubic structures as a function of Y_2O_3 concentration. To maintain charge neutrality an oxygen vacancy is created to compensate the negative charge induced, by every two Y^{3+} ions substituting for a pair of Zr^{4+} ions. Open symbols in Fig. 2a are *a* and *c* lattice parameters from the XRD literature [13, 58–63], closed symbols are corresponding values from our laboratory. The *t*-ZrO_2 tetragonality ratio c_t/a_t diminishes with increasing Y_2O_3 concentration (i.e. the lattice parameters become closer to cubic zirconia) until it reaches unity at ~ 14.8 wt% or 8.2 mol% Y_2O_3 concentration. The corresponding unit cell volumes V_c and V_t in Fig. 2b, evaluated using best-fit lines in Fig 2a, increase with increasing Y concentration up to the *t*–*c* transition point. Note that the rate of increase is significantly higher for *t*-ZrO_2 relative to *c*-ZrO_2.

2.2 Density

A model for the calculation of the cubic lattice constants and subsequently the theoretical density of ZrO_2 single crystals with different amounts of stabilizing elements was developed by Aleksandrov et al. (1976) [57]. That model was based on the assumption of spherical packing of ions while folding in the calculated mean number of anion vacancies per unit cell. Later, Ingel and Lewis extended the Aleksandrov model to calculate lattice parameters and theoretical densities of cubic and tetragonal single-phase ZrO_2-Y_2O_3 compositions, and validated the theoretical predictions with experimental data from their laboratories and from the available literature [58]. Following Ingel and Lewis's analysis, the theoretical densities for single-phase polycrystalline *t*- or *c*-ZrO_2 stabilized with 3, 4, and 5 mol% Y_2O_3 are shown in Table I. As can be seen, the density of both forms of zirconia decreases as the Y_2O_3 content increases. This functional dependence is to be expected since as the Y_2O_3 concentration increases there is an increase in attendant oxygen vacancies and unit cell volume.

The values listed in Table 1 serve as a starting point to derive theoretical densities of ZrO_2–Y_2O_3 solid solutions with any composition of mixed *c* and *t* phases. We utilize a classic rule of mixtures

$$\rho = \rho_t V_t + \rho_c V_c \quad (1)$$

where ρ_t and ρ_c are densities and V_t and V_c are volume fractions. Theoretical densities of 3Y, 4Y, and 5YSZ using Eq. 1 in combination with the data shown in Table 1 are plotted in Fig. 3 as a function of cubic phase content (both in vol% V_c and wt% M_c).

3. Materials and Methods

Disc-shaped specimens 13 mm diameter and 1 mm thickness were prepared from pre-sintered 3YSZ (Zpex), 4YSZ (Zpex 4) and 5YSZ (Zpex Smile) zirconia rods (Tosoh Corporation, Tokyo, Japan). These pre-sintered zirconia rods were fabricated by bisque firing of cold-isostatically pressed powders at 940°C. The surface of each biscuit disc was hand ground after cutting, using silicon carbide abrasive papers ranging from 320 to 1200 grits [64]. A total of 216 discs were prepared for this study. Nine specimens from each composition were sintered at 1100, 1200, 1300, 1350, 1400, 1450, 1500, and 1550 °C, bridging the temperature range for biscuit firing through to sintering of commercial dental zirconias. In all cases, a constant heating and cooling rate of 8°C per min with a dwell time of 2 h was employed. Opposite surfaces of the sintered zirconia discs were polished with successively finer grits down to 0.5 μm diamond suspension, using an automatic polishing machine under water irrigation (Ecomet 4, Buehler, Lake bluff, IL, USA).

Precursor dilatometric measurements (L75VD1600, Linseis Inc., Robbinsville, NJ, USA) were made on green rods of the three YSZ materials. Sintered specimens were analyzed by X-ray diffraction (X'Pert3 Powder, PANalytical, Netherlands) in order to identify crystalline phase contents (CuKα radiation). Specimens were mounted on the sample stage with the top side against the flat surface of a stub. Step scanning conditions were set at a fixed interval 0.01° and rate 0.3 s over a diffraction angle range 2Θ = 20° to 80° [65]. A full-profile fitting refinement method was used to calculate the phase fractions of each material via the Rietveld method using HighScore Plus software [66]. Bulk densities ρ_{Bulk} were measured using a density kit accessory and analytical balance (Mettler Toledo, Columbus, OH, USA) at room temperature via Archimedes' principle [67]. The relative density of ceramic specimens was determined using $\rho_{Rel} = (\rho_{Bulk}/\rho_{Theo})$ x 100%, with theoretical density ρ_{Theo} calculated from the tetragonal and cubic content for the different YSZ compositions in Fig. 3.

Strengths were measured using a piston-on-three-ball biaxial flexure test fixture on a universal testing machine (Instron 5566, Instron, Norwood, MA, USA) at 1 mm/min crosshead speed. The disc specimens were supported by three hardened steel balls 120° apart on a support circle of diameter 4 mm, with piston diameter 1.4 mm. Strength S was calculated from the fracture load using the standard equation described in ISO 6872/2015 [68].

Specimen translucencies were measured using a dental colorimeter (SpectroShade Micro, MHT, Niederhasli, Switzerland). Color coordinates CIEL*a*b* [69] were measured over standard backgrounds (black L* = 1.8, a* = 1.3, b* = −1.5 and white L* = 95.7, a* = −1.3, b* = 2.6). To ensure optical continuity, a drop of coupling liquid (refractive index: 1.8, Gem Refractometer Liquid, Cargille Laboratories, Inc., Cedar Grove, NJ, USA) was placed between the specimen and background. Translucency parameters were determined by the color difference between the specimen on black (B) and white (W) backgrounds, using the following equation [70]

$$TP = \sqrt{\left(L_B^* - L_W^*\right)^2 + \left(a_B^* - a_W^*\right)^2 + \left(b_B^* - b_W^*\right)^2}$$

where L*, a*, and b* refer respectively to the lightness, redness to greenness, and yellowness to blueness coordinates in the CIE color space [69].

Microstructural quantification was carried out on two YSZ specimens from each group. These specimens were thermally etched at 1050°C for 20 min at heating and cooling rates of 10°C per min. Surfaces were coated with a nanometric layer of gold-palladium prior to imaging in a Field Emission Scanning Electron Microscope (Quanta 250 FEG, Thermo Fisher Scientific, Waltham, MA, USA). Grain sizes were measured from SEM micrographs using the linear intercept technique [71], covering at least 500 grains per specimen [72] and with a ‘correction factor’ of 1.56 for truncated octahedral shaped grains [73].

4. Results

4.1 Material characterization

Relative densities of 3YSZ, 4YSZ, and 5YSZ are plotted in Fig. 4 as a function of sintering temperature. 3YSZ began to densify at a lower temperature relative to 4YSZ and 5YSZ and reached ~99% of its theoretical density at 1300°C. The other compositions achieved that density above 1350°C. Dilatometric measurements on green rods showed major volume shrinkage around 1025°C for 3YSZ, 1050°C for 4YSZ, and 1070°C for 5YSZ, consistent with the trends in Fig. 4.

Figure 5 shows the cubic phase weight fraction for the three YSZ compositions as a function of sintering temperature. All three compositions exhibited a similar trend of increasing transformation from t-ZrO_2 to c-ZrO_2 with increasing temperature, more rapidly above 1350°C. The transformation rate for 3YSZ was higher than 4YSZ and even more so than 5YSZ.

Figure 6 shows polished and thermally etched surfaces of 3YSZ, 4YSZ and 5YSZ compositions after sintering at 1100°C, 1300°C and 1500°C. High density smooth surfaces were attained above 1300°C, consistent with the relative density measurements in Fig. 4. Note the accelerated grain growth for all compositions above this temperature. Grain morphologies were equi-axed in all cases. Figure 7 shows that grain size d remained below 1 μm over the sintering range, except in 5YSZ at temperatures above 1450°C. Error bars represent one standard deviation of the mean.

4.2 Mechanical and optical properties

Figure 8 plots biaxial flexural strength S of the three YSZ compositions as a function of (a) sintering temperature, (b) *c*-ZrO_2 content, and (c) grain size *d*. Error bars represent one standard deviation of the mean. The ranking of materials from high to low was 3YSZ, 4YSZ and 5YSZ. Strength in all cases increased steadily with sintering temperature up to ~ 1350°C in Fig. 8a, corresponding to the point at which 99% relative density was achieved. Beyond that temperature the strengths of 3YSZ and 4YSZ continued to increase, but gradually, revealing some tolerance to sintering condition. The ultimate strengths in all three YSZ materials are broadly acceptable for clinical purposes [74, 75], although 5YSZ, the composition with most *c*-ZrO_2 content, presents as the least durable. The role of cubic content on *S* is seen more clearly in Fig. 8b. Here, in order to rule out the effect of porosity, only compositions with a relative density ≥ 99% (i.e. sintered at ≥ 1350°C) are compared. The dependence is not strong for any of the compositions, but is particularly insensitive in the case of 5YSZ. The plot of *S* as a function of grain size *d* in Fig. 8c, again for compositions sintered at ≥ 1350°C, shows similar insensitivities. It all points to a certain tolerance of YSZ ceramics to variations in the sintering process.

In analogy to Fig. 8, Fig. 9 plots translucency parameter TP as functions of the same variables, i.e. (a) sintering temperature, (b) *c*-ZrO_2 content, and (c) grain size. Again, error bars represent one standard deviation of the mean. In contrast to strength, Fig. 9a indicates that a higher sintering temperature, closer to 1400°C than 1350°C, was required to achieve an elevated *TP*. Moreover, *TP* continued to increase at sintering temperatures up to 1550°C, especially in 5YSZ. This is consistent with the recommendations of dental manufacturers, that their zirconia products be sintered above 1400°C. Accordingly, the plots of *TP* as a function of cubic content in Fig. 9b and grain size in Fig. 9c are shown for materials with an elevated *TP* (i.e. sintered at ≥ 1400°C). It is apparent that the translucency of all YSZ compositions increases with both cubic content and grain size.

Finally, Fig. 10 examines correlations between strength *S* and translucency *TP* for the three YSZ materials. Error bars represent one standard deviation of the mean ($n = 9$). Again, to rule out any effects of porosity on *S* and *TP*, only compositions with > 99% relative density and an elevated *TP* (i.e. sintered at temperatures ≥ 1400°C) are included here. Tellingly, *S* actually increased with *TP* in both 3YSZ and 4YSZ, but showed no significant dependence in 5YSZ. This trend appears to be counter to common lore, and presages a processing route where both mechanical integrity and optical esthetics may be achieved concurrently.

5. Discussion

5.1 Crystallography and microstructure

The development of strong and esthetic zirconias, primarily for use as dental restorative ceramics, has centered around the stabilizing role of yttria additives in crystallographic and microstructural properties. Essential crystallography has been described in Figs. 1 and 2. There is a range of compositional variants, but most attention has been given to 3YSZ, 4YSZ and 5YSZ. In these compositions Zr^{4+} ions are substituted by Y^{3+}, balanced by the formation of oxygen O^{2-} vacancies. As seen in Fig. 2, increasing dopant concentration

diminishes the unit cell ratio c/a in the tetragonal phase t-ZrO_2, with attendant changes in the unit cell volumes, until at ~ 8 mol% the lattice parameters approach those of the cubic phase at $c/a = 1$. In higher concentrations the material transitions fully to c-ZrO_2. This transition is firmly supported by direct experimental observations [13, 50, 58, 59] as well as by calculations based on density-function theory [76, 77]. Lattice shrinkage in t-ZrO_2 along the c-axis reduces not only tetragonality but also Zr–O bond length, ultimately rendering YSZ more thermodynamically stable [49].

We have used a simple rule of mixtures model to calculate the theoretical density of t and c biphasic YSZ material (Fig. 3), enabling computation of *relative* density from bulk density measurements (Fig. 4). We have seen that the unit cell volumes of t-ZrO_2 and c-ZrO_2 increase with Y^{3+} dopant content (Fig. 2b). Substituting Zr with the lighter element Y while removing O for charge neutrality decreases the molar mass of YSZ. These, along with an increasing unit cell volume with Y concentration, ultimately account for diminishing densities with increasing dopant content (Fig. 3).

Especially important is the role of sintering conditions on the zirconia microstructures. As seen in Fig. 4, all zirconias attained 99% of their theoretical densities after sintering to 1350°C (Fig. 4). Above ~ 1400°C the content of the cubic phase c-ZrO_2 continues to increase (Fig. 5) and grain growth ensues (Figs. 6 and 7). In a typical ceramic sintering process the powder compact shrinks while much of the porosity is eliminated. Initially, neck formation between powder particulates accounts for ~ 3 vol% of the shrinkage. Subsequently, formation of interconnecting pore channels and multi-grain junctions increases shrinkage by a further 93% [78, 79]. Finally, all three YSZ compositions sintered at temperatures ≥ 1350°C enter the final stage of densification as interconnected pore channels collapse into isolated pores. This last stage triggers accelerates grain boundary migration and thus grain growth [79–82]. Grain boundary mobility responsible for the accelerated grain growth increases further with increasing sintering temperature [83], particularly in 5YSZ (Fig. 7). Enhanced grain boundary mobility has also been associated with an increased Y^{3+} ion diffusion rate, facilitating transformation into c-ZrO_2 [84].

5.2 Strength and translucency

Building on the description of crystallographic and microstructural evolution of YSZ ceramics, we are now in a position to examine the role of Y^{3+} dopant (and O^{2-} vacancy) in the strength and translucency properties of YSZ.

The strength increases with sintering temperature observed for all YSZ variants (Fig. 8a) are readily correlated with near-full densification above 1350°C, i.e. elimination of microstructural pores and defects. The dependence on cubic phase content (Fig. 8b) can be ascribed to differences in toughness [21, 85]. The toughness of YSZ ceramics may not be high (< 5 $MPa.m^{1/2}$) by wider material standards [21], but nevertheless is enhanced via limited tetragonal to monoclinic transformation [85]. The degree of $t \rightarrow m$ transformation in turn depends on the crystallography. As alluded to earlier, the lattice distortion of the tetragonal crystal structure decreases with the concentration of Y^{3+} cations, observed most notably in a reduction in the c-axis, in turn manifested as a reduction in the Zr–O bond length. The latter reduction compromises the $t \rightarrow m$ capacity of YSZ, thus reducing

strength. As a corollary, the same reduction renders the material less susceptible to low temperature degradation [86, 87]. It is noteworthy that strength shows little sensitivity to grain size (Fig. 8c), especially in 5YSZ, implying strong grain boundaries (transgranular fracture). Regardless of the dopant content, the strengths of the zirconia compositions rank from higher to lower in the order 3YSZ, 4YSZ and 5YSZ. In short, the mechanical properties of YSZ are governed by both crystallography and microstructure.

It has been well-established that translucency of polycrystalline ceramics is governed by refractive index, birefringence, and grain size [88, 89]. A larger grain size yields higher translucency. Lower refractive index and smaller birefringence are also factors in higher translucency. Refractive index decreases with density, whereas birefringence in *t*-ZrO_2 decreases as the lattice parameter ratio c/a decreases [88, 89]. As a result, the translucency of YSZ increases drastically with the Y^{3+} content (Figs. 2 and 3) and sintering temperature (Fig. 9). Above 1350°C isotropic *c*-ZrO_2 is optically transparent, thereby increasing translucency in proceeding from 3YSZ through to 5YSZ (Fig. 5).

From a clinical perspective, strength and translucency are vital, if sometimes conflicting, considerations. Across the three YSZ compositions examined, 3YSZ is intrinsically stronger than 4YSZ, more so than 5YSZ (Fig. 8), whereas 5YSZ is more translucent than 4YSZ and 3YSZ (Fig. 9). This is widely reported in both dental and materials science literature as a conflicting trend [21, 90]. In this context, the most intriguing finding of the current study is that, individually, the strengths of densely sintered 3YSZ and 4YSZ actually increase with translucency, while strength in 5YSZ remains undiminished (Fig. 10). The question then is generally posed as to how one may improve the translucency of 3YSZ without compromising its strength, or alternatively, how to improve the strength of 4YSZ and 5YSZ without sacrificing translucency. The current findings have significant clinical implications, as for any given YSZ composition it is now potentially possible to improve translucency and strength concurrently. The key to an explanation would appear to lie in the optimization of material processing conditions in order to produce functional crystal structures and defect-free microstructures. We continue to work on both these fronts.

6. Conclusions

- Strength and translucency of biphasic zirconia bioceramics depend on crystallography and microstructure.
- The strength of YSZ ceramics decreases, translucency increases, with yttria content.
- Microstructures of YSZ, notably grain sizes, are governed by densification above a critical sintering temperature.
- Critically, the potential for optimization of YSZ ceramics, whereby both strength and translucency may be improved concurrently, is demonstrable.

Acknowledgements

The authors wish to thank Dr. Brian R. Lawn for discussions throughout the preparation of this manuscript. This work was supported by the U.S. National Institutes of Health/National Institute of Dental and Craniofacial Research

(grant numbers R01DE026279 and R01DE026772). This work was carried out in part at the Singh Center for Nanotechnology, which is supported by the NSF National Nanotechnology Coordinated Infrastructure Program under grant NNCI-2025608. The funding sources had no involvement in study design; data collection, analysis and interpretation; manuscript writing; and decision to submit the article for publication.

References

[1]. McCullough JD, Trueblood KN, The crystal structure of baddeleyite (monoclinic ZrO_2), Acta Crystallogr. 12(7) (1959) 507–511.

[2]. Teufer G, The crystal structure of tetragonal ZrO_2, Acta Crystallogr. 15(11) (1962) 1187–1187.

[3]. Wolten GM, Diffusionless phase transformations in zirconia and hafnia, J. Am. Ceram. Soc 46(9) (1963) 418–422.

[4]. Zhang Y, Chen H-X, Duan L, Fan J-B, Ni L, Ji V, A comparison study of the structural and mechanical properties of cubic, tetragonal, monoclinic, and three orthorhombic phases of ZrO_2, J. Alloys Compd 749 (2018) 283–292.

[5]. Leger JM, Tomaszewski PE, Atouf A, Pereira AS, Pressure-induced structural phase transitions in zirconia under high pressure, Phys. Rev. B 47(21) (1993) 14075–14083.

[6]. Ohtaka O, Yamanaka T, Kume S, Hara N, Asano H, Izumi F, Structural analysis of orthorhombic hafnia by neutron powder diffraction, J. Am. Ceram. Soc 78(1) (1995) 233–237.

[7]. Block S, da Jornada JAH, Piermarini GJ, Pressure-temperature phase diagram of zirconia, J. Am. Ceram. Soc 68(9) (1985) 497–499.

[8]. Liu L-G, New high pressure phases of ZrO_2 and HfO_2, J. Phys. Chem. Solids 41(4) (1980) 331–334.

[9]. Kisi EH, Howard CJ, Hill RJ, Crystal structure of orthorhombic zirconia in partially stabilized zirconia, J. Am. Ceram. Soc 72(9) (1989) 1757–1760.

[10]. Kelly JR, Denry I, Stabilized zirconia as a structural ceramic: An overview, Dent. Mater 24(3) (2008) 289–98. [PubMed: 17624420]

[11]. Porter DL, Heuer AH, Microstructural development in MgO-partially stabilized zirconia (Mg-PSZ), J. Am. Ceram. Soc 62(5–6) (1979) 298–305.

[12]. Garvie RC, Nicholson PS, Structure and thermomechanical properties of partially stabilized zirconia in the CaO-ZrO_2 system, J. Am. Ceram. Soc 55(3) (1972) 152–157.

[13]. Scott HG, Phase relationships in the zirconia-yttria system, J. Mater. Sci 10(9) (1975) 1527–1535.

[14]. Duwez P, Odell F, Phase relationships in the system zirconia—ceria, J. Am. Ceram. Soc 33(9) (1950) 274–283.

[15]. Ahmadi-Pidani R, Shoja-Razavi R, Mozafarinia R, Jamali H, Evaluation of hot corrosion behavior of plasma sprayed ceria and yttria stabilized zirconia thermal barrier coatings in the presence of Na_2SO_4+V_2O_5 molten salt, Ceram. Int 38(8) (2012) 6613–6620.

[16]. Di Girolamo G, Blasi C, Schioppa M, Tapfer L, Structure and thermal properties of heat treated plasma sprayed ceria–yttria co-stabilized zirconia coatings, Ceram. Int 36(3) (2010) 961–968.

[17]. Duwez P, Odell F, Brown FH Jr., Stabilization of zirconia with calcia and magnesia, J. Am. Ceram. Soc 35(5) (1952) 107–113.

[18]. Garvie RC, Hannink RH, Pascoe RT, Ceramic steel?, Nature 258(5537) (1975) 703–704.

[19]. Wilk GD, Wallace RM, Anthony JM, High-κ gate dielectrics: Current status and materials properties considerations, J. Appl. Phys 89(10) (2001) 5243–5275.

[20]. Zhang Q, Shen J, Wang J, Wu G, Chen L, Sol–gel derived ZrO_2–SiO_2 highly reflective coatings, Int. J. Inorg. Mater 2(4) (2000) 319–323.

[21]. Zhang Y, Lawn BR, Novel zirconia materials in dentistry, J. Dent. Res 97(2) (2018) 140–147. [PubMed: 29035694]

[22]. Stapper G, Bernasconi M, Nicoloso N, Parrinello M, Ab initio study of structural and electronic properties of yttria-stabilized cubic zirconia, Phys. Rev. B 59(2) (1999) 797–810.

[23]. Zhao X, Vanderbilt D, Phonons and lattice dielectric properties of zirconia, Phys. Rev. B 65(7) (2002) 075105.

[24]. Hsu SM, Shen MC, Ceramic wear maps, Wear 200(1) (1996) 154–175.

[25]. Arima T, Yamasaki S, Yamahira K, Idemitsu K, Inagaki Y, Degueldre C, Evaluation of thermal conductivity of zirconia-based inert matrix fuel by molecular dynamics simulation, J. Nucl. Mater 352(1) (2006) 309–317.

[26]. Butler EP, Transformation-toughened zirconia ceramics, Mater. Sci. Technol 1(6) (1985) 417–432.

[27]. Hannink RHJ, Stringer RK, Swain MV, The development of zirconia transformation toughened ceramics in Australia, J. Aus. Ceram. Soc 50(1) (2014) 1–14.

[28]. The use of zirconia as a refractory material, Nature 99(2488) (1917) 375–376.

[29]. Zhou X, Balachov I, Macdonald DD, The effect of dielectric coatings on IGSCC in sensitized type 304 ss in high temperature dilute sodium sulfate solution, Corros. Sci 40(8) (1998) 1349–1362.

[30]. Clarke DR, Phillpot SR, Thermal barrier coating materials, Mater. Today 8(6) (2005) 22–29.

[31]. Wright PK, Evans AG, Mechanisms governing the performance of thermal barrier coatings, Curr. Opin. Solid State Mater. Sci 4(3) (1999) 255–265.

[32]. Singhal SC, Advances in solid oxide fuel cell technology, Solid State Ion. 135(1) (2000) 305–313.

[33]. Yamamoto O, Solid oxide fuel cells: Fundamental aspects and prospects, Electrochim. Acta 45(15) (2000) 2423–2435.

[34]. Ramamoorthy R, Dutta PK, Akbar SA, Oxygen sensors: Materials, methods, designs and applications, J. Mater. Sci 38(21) (2003) 4271–4282.

[35]. Casolco SR, Xu J, Garay JE, Transparent/translucent polycrystalline nanostructured yttria stabilized zirconia with varying colors, Scr. Mater 58(6) (2008) 516–519.

[36]. Piconi C, Maccauro G, Zirconia as a ceramic biomaterial, Biomaterials 20(1) (1999) 1–25. [PubMed: 9916767]

[37]. Denry I, Kelly JR, State of the art of zirconia for dental applications, Dent. Mater 24(3) (2008) 299–307. [PubMed: 17659331]

[38]. Zhang Y, Kelly JR, Dental ceramics for restoration and metal veneering, Dent. Clin. North. Am 61(4) (2017) 797–819. [PubMed: 28886769]

[39]. Sailer I, Makarov NA, Thoma DS, Zwahlen M, Pjetursson BE, All-ceramic or metal-ceramic tooth-supported fixed dental prostheses (FDPs)? A systematic review of the survival and complication rates. Part I: Single crowns (SCs), Dent. Mater 31(6) (2015) 603–23. [PubMed: 25842099]

[40]. Sailer I, Fehér A, Filser F, Gauckler LJ, Lüthy H, Hämmerle CH, Five-year clinical results of zirconia frameworks for posterior fixed partial dentures, Int. J. Prosthodont 20(4) (2007) 383–8. [PubMed: 17695869]

[41]. Manicone PF, Rossi Iommetti P, Raffaelli L, An overview of zirconia ceramics: Basic properties and clinical applications, J. Dent 35(11) (2007) 819–26. [PubMed: 17825465]

[42]. Kolakarnprasert N, Kaizer MR, Kim DK, Zhang Y, New multi-layered zirconias: Composition, microstructure and translucency, Dent. Mater 35(5) (2019) 797–806. [PubMed: 30853208]

[43]. Denry I, Abdelaal M, Dawson DV, Holloway JA, Kelly JR, Effect of crystalline phase assemblage on reliability of 3Y-TZP, J. Prosthet. Dent (2020).

[44]. Amat NF, Muchtar A, Amril MS, Ghazali MJ, Yahaya N, Effect of sintering temperature on the aging resistance and mechanical properties of monolithic zirconia, J. Mater. Res. Technol 8(1) (2019) 1092–1101.

[45]. Ruiz L, Readey MJ, Effect of heat treatment on grain size, phase assemblage, and mechanical properties of 3 mol% Y-TZP, J. Am. Ceram. Soc 79(9) (1996) 2331–2340.

[46]. Stawarczyk B, Özcan M, Hallmann L, Ender A, Mehl A, Hämmerlet CHF, The effect of zirconia sintering temperature on flexural strength, grain size, and contrast ratio, Clin. Oral Investig 17(1) (2013) 269–274.

[47]. Jiang L, Liao Y, Wan Q, Li W, Effects of sintering temperature and particle size on the translucency of zirconium dioxide dental ceramic, J. Mater. Sci. Mater. Med 22(11) (2011) 2429–2435. [PubMed: 21922331]

[48]. Ersoy NM, Aydoğdu HM, Değirmenci BÜ, Çökük N, Sevimay M, The effects of sintering temperature and duration on the flexural strength and grain size of zirconia, Acta Biomater. Odontol. Scand 1(2–4) (2015) 43–50. [PubMed: 28642900]

[49]. Pan Y, Influence of oxygen vacancies on the electronic and optical properties of zirconium dioxide from first-principles calculations, J. Electron. Mater 48(8) (2019) 5154–5160.

[50]. Raza M, Cornil D, Cornil J, Lucas S, Snyders R, Konstantinidis S, Oxygen vacancy stabilized zirconia (OVSZ); a joint experimental and theoretical study, Scr. Mater 124 (2016) 26–29.

[51]. Sekhar PK, Brosha EL, Mukundan R, Nelson MA, Toracco D, Garzon FH, Effect of yttria-stabilized zirconia sintering temperature on mixed potential sensor performance, Solid State Ion. 181(19) (2010) 947–953.

[52]. Zhang H, Kim B-N, Morita K, Keijiro Hiraga HY, Sakka Y, Effect of sintering temperature on optical properties and microstructure of translucent zirconia prepared by high-pressure spark plasma sintering, Sci. Technol. Adv. Mater 12(5) (2011) 055003. [PubMed: 27877441]

[53]. Paygin VD, Stepanov S, Dvilis E, Khasanov O, Alishin T, Valiev D, Effect of technological parameters on optical and mechanical properties of spark plasma sintered transparent YSZ ceramics, Ceram. Int 47 (2021) 11169–11175.

[54]. Xia X, Oldman R, Catlow R, Computational modeling study of bulk and surface of yttria-stabilized cubic zirconia, Chem. Mater 21(15) (2009) 3576–3585.

[55]. Grambow J, Wille S, Kern M, Impact of changes in sintering temperatures on characteristics of 4YSZ and 5YSZ, J. Mech. Behav. Biomed. Mater 120 (2021) 104586. [PubMed: 34044252]

[56]. Fonseca YR, Elias CN, Monteiro SN, dos Santos HES, dos Santos C, Modeling of the influence of chemical composition, sintering temperature, density, and thickness in the light transmittance of four zirconia dental prostheses, Materials 12(16) (2019) 2529. [PubMed: 31398941]

[57]. Aleksandrov VI, Bal'yano GE, Lukin BV, Structure of monocrystals of stabilized zirconium dioxide, Izv. Akad. Nauk SSSR, Neorg. Mater. (USSR) 12(2) (1976) 273–277.

[58]. Ingel RP, Lewis D, Lattice Parameters and Density for Y_2O_3-Stabilized ZrO_2, J. Am. Ceram. Soc 69(4) (1986) 325–332.

[59]. Krogstad JA, Lepple M, Gao Y, Lipkin DM, Levi CG, Effect of yttria content on the zirconia unit cell parameters, J. Am. Ceram. Soc 94(12) (2011) 4548–4555.

[60]. Brandon JR, Taylor R, Phase stability of zirconia-based thermal barrier coatings part I. Zirconia-yttria alloys, Surf. Coat. Technol 46(1) (1991) 75–90.

[61]. Toraya H, Effect of $YO_{1.5}$ Dopant on unit-cell parameters of ZrO_2 at low contents of $YO_{1.5}$, J. Am. Ceram. Soc. 72(4) (1989) 662–664.

[62]. Pascual C, Durán P, Subsolidus phase equilibria and ordering in the system ZrO_2-Y_2O_3, J. Am. Ceram. Soc 66(1) (1983) 23–27.

[63]. Borik MA, Borichevskij VP, Bublik VT, Kulebyakin AV, Lomonova EE, Milovich FO, Myzina VA, Ryabochkina PA, Sidorova NV, Tabachkova NY, Anisotropy of the mechanical properties and features of the tetragonal to monoclinic transition in partially stabilized zirconia crystals, J. Alloys Compd 792 (2019) 1255–1260.

[64]. Borba M, Okamoto TK, Zou M, Kaizer MR, Zhang Y, Damage sensitivity of dental zirconias to simulated occlusal contact, Dent. Mater 37(1) (2021) 158–167. [PubMed: 33234315]

[65]. Vardhaman S, Borba M, Kaizer MR, Kim D, Zhang Y, Wear behavior and microstructural characterization of translucent multilayer zirconia, Dent. Mater 36(11) (2020) 1407–1417. [PubMed: 32958309]

[66]. Mao L, Kaizer MR, Zhao M, Guo B, Song YF, Zhang Y, Graded ultra-translucent zirconia (5Y-PSZ) for strength and functionalities, J. Dent. Res 97(11) (2018) 1222–1228. [PubMed: 29694258]

[67]. ASTM C20-00, Standard test methods for apparent porosity, water absorption, apparent specific gravity, and bulk density of burned refractory brick and shapes by boiling water, ASTM International, West Conshohocken, PA, 2018.

[68]. Luz JN, Kaizer M.d.R., Ramos N.d.C., Anami LC, Thompson VP, Saavedra GSFA, Zhang Y, Novel speed sintered zirconia by microwave technology, Dent. Mater 37(5) (2021) 875–881. [PubMed: 33715863]

[69]. CIE, Technical Committee: Colorimetry, CIE pub no 15.3. Vienna, Austria: CIE Central Bureau (2004).

[70]. Yan J, Kaizer MR, Zhang Y, Load-bearing capacity of lithium disilicate and ultra-translucent zirconias, J. Mech. Behav. Biomed. Mater 88 (2018) 170–175. [PubMed: 30173069]

[71]. ASTM Standard E112, Standard test methods for determining average grain size, ASTM International, West Conshohocken, PA, 2013.

[72]. Tong H, Tanaka CB, Kaizer MR, Zhang Y, Characterization of three commercial Y-TZP ceramics produced for their high-translucency, high-strength and high-surface area, Ceram. Int 42(1) (2016) 1077–1085. [PubMed: 26664123]

[73]. Wurst JC, Nelson JA, Lineal intercept technique for measuring grain size in two-phase polycrystalline ceramics, J. Am. Ceram. Soc 55(2) (1972) 109–109.

[74]. Solá-Ruiz MF, Baixauli-López M, Roig-Vanaclocha A, Amengual-Lorenzo J, Agustín-Panadero R, Prospective study of monolithic zirconia crowns: clinical behavior and survival rate at a 5-year follow-up, J. Prosthodont. Res 65(3) (2021) 284–290. [PubMed: 33041280]

[75]. Sulaiman TA, Abdulmajeed AA, Delgado A, Donovan TE, Fracture rate of 188695 lithium disilicate and zirconia ceramic restorations after up to 7.5 years of clinical service: A dental laboratory survey, J. Prosthet. Dent 123(6) (2020) 807–810. [PubMed: 31703926]

[76]. Mráz S, Schneider JM, Influence of the negative oxygen ions on the structure evolution of transition metal oxide thin films, J. Appl. Phys 100(2) (2006) 023503.

[77]. Severin D, Sarakinos K, Kappertz O, Pflug A, Wuttig M, Tailoring of structure formation and phase composition in reactively sputtered zirconium oxide films using nitrogen as an additional reactive gas, J. Appl. Phys 103(8) (2008) 083306.

[78]. Kang SJL, Sintering: Densification, grain growth and microstructure, 2005.

[79]. Coble RL, Sintering crystalline solids. I. Intermediate and final state diffusion models, in: Sōmiya S, Moriyoshi Y (Eds.), Sintering Key Papers, Springer Netherlands, Dordrecht, 1990, pp. 55–67.

[80]. Nichols FA, Mullins WW, Surface- (interface-) and volume-diffusion contributions to morphological changes driven by capillarity, The American Institute of Mining, Metallurgical, and Petroleum Engineers, 1965.

[81]. Hassold GN, Chen I-W, Srolovitz DJ, Computer simulation of final-stage sintering: I, model kinetics, and microstructure, J. Am. Ceram. Soc 73(10) (1990) 2857–2864.

[82]. Chen I-W, Hassold GN, Srolovitz DJ, Computer simulation of final-stage sintering: II, Influence of initial pore size, J. Am. Ceram. Soc 73(10) (1990) 2865–2872.

[83]. Park J-K, Kim D-Y, Effect of grain size on diffusion-induced grain-boundary migration in $Ba(Zn_{1/3}Nb_{2/3})O_3$ ceramics, J. Am. Ceram. Soc 79(5) (1996) 1405–1408.

[84]. Matsui K, Horikoshi H, Ohmichi N, Ohgai M, Yoshida H, Ikuhara Y, Cubic-formation and grain-growth mechanisms in tetragonal zirconia polycrystal, J. Am. Ceram. Soc 86(8) (2003) 1401–1408.

[85]. Hannink RHJ, Kelly PM, Muddle BC, Transformation toughening in zirconia-containing ceramics, J. Am. Ceram. Soc 83(3) (2000) 461–487.

[86]. Chevalier J, Gremillard L, Deville S, Low-temperature degradation of zirconia and implications for biomedical implants, Annu. Rev. Mater. Res 37(1) (2007) 1–32.

[87]. Chevalier J, Gremillard L, Virkar AV, Clarke DR, The tetragonal-monoclinic transformation in zirconia: lessons learned and future trends, J. Am. Ceram. Soc 92(9) (2009) 1901–1920.

[88]. Zhang Y, Making yttria-stabilized tetragonal zirconia translucent, Dent. Mater 30(10) (2014) 1195–1203. [PubMed: 25193781]

[89]. Zhao M, Sun Y, Zhang J, Zhang Y, Novel translucent and strong submicron alumina ceramics for dental restorations, J. Dent. Res 97(3) (2018) 289–295. [PubMed: 28977778]

[90]. Zhang F, Reveron H, Spies BC, Van Meerbeek B, Chevalier J, Trade-off between fracture resistance and translucency of zirconia and lithium-disilicate glass ceramics for monolithic restorations, Acta Biomater. 91 (2019) 24–34. [PubMed: 31034947]

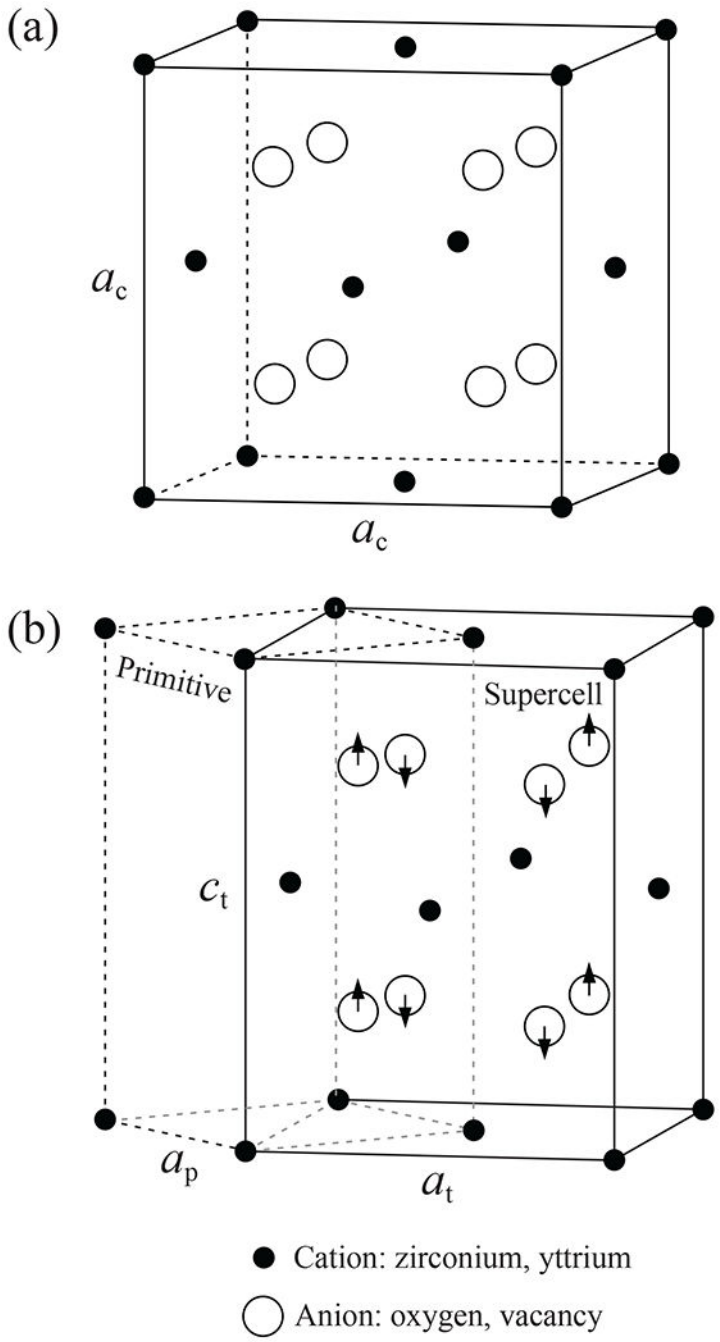

Figure 1.
Crystallography of zirconia, (a) cubic and (b) tetragonal. Small closed spheres indicate zirconium or yttrium cations, large open symbols indicate oxygen anions and/or vacancy. Arrows in (b) indicate atomic displacements in tetragonal structure. Solid lines in (a) represent unit cell, in (b) equivalent supercell. Dashed lines in (b) represent primitive cell.

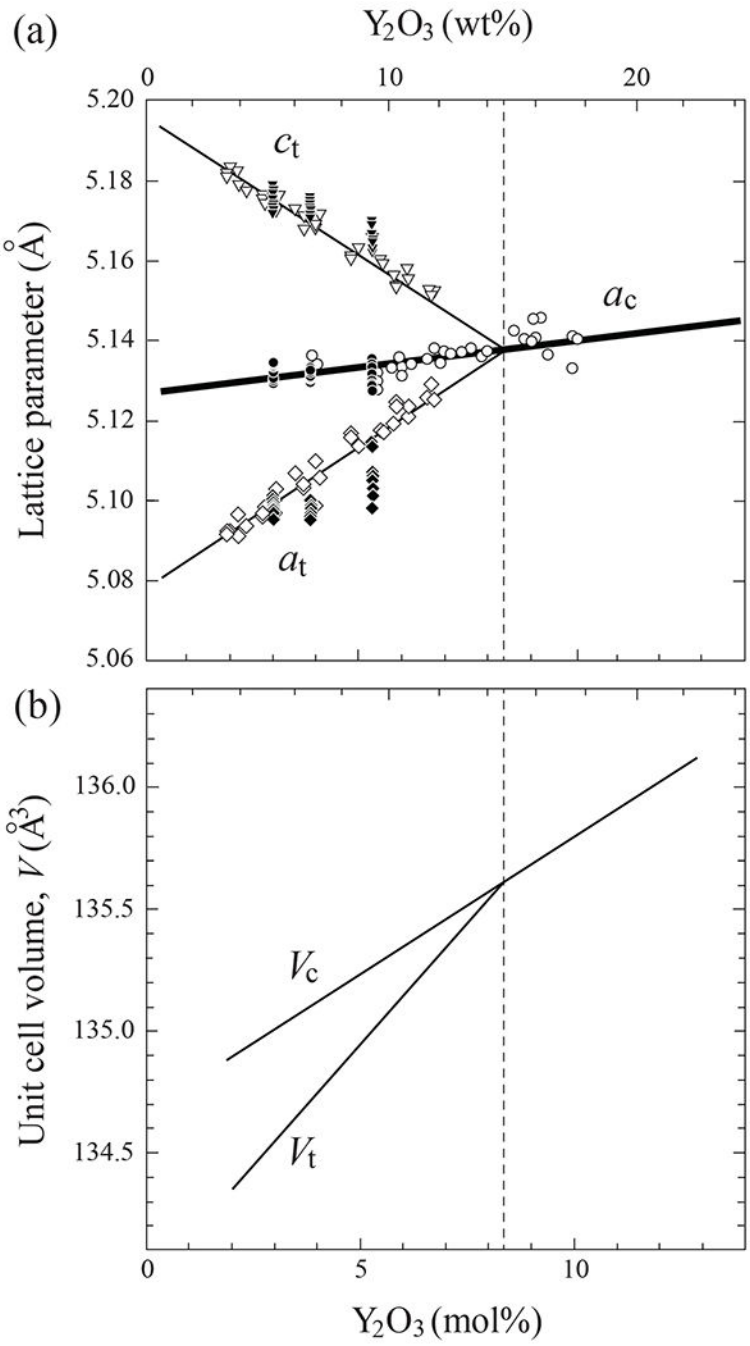

Figure 2.

Plots of (a) lattice parameter and (b) cell volume for ZrO_2 with Y_2O_3 dopant. Data from literature (open symbols) [13, 58–63] and current work (closed symbols). Transformation from tetragonal to cubic phase occurs at 8.2 mol% Y_2O_3 content.

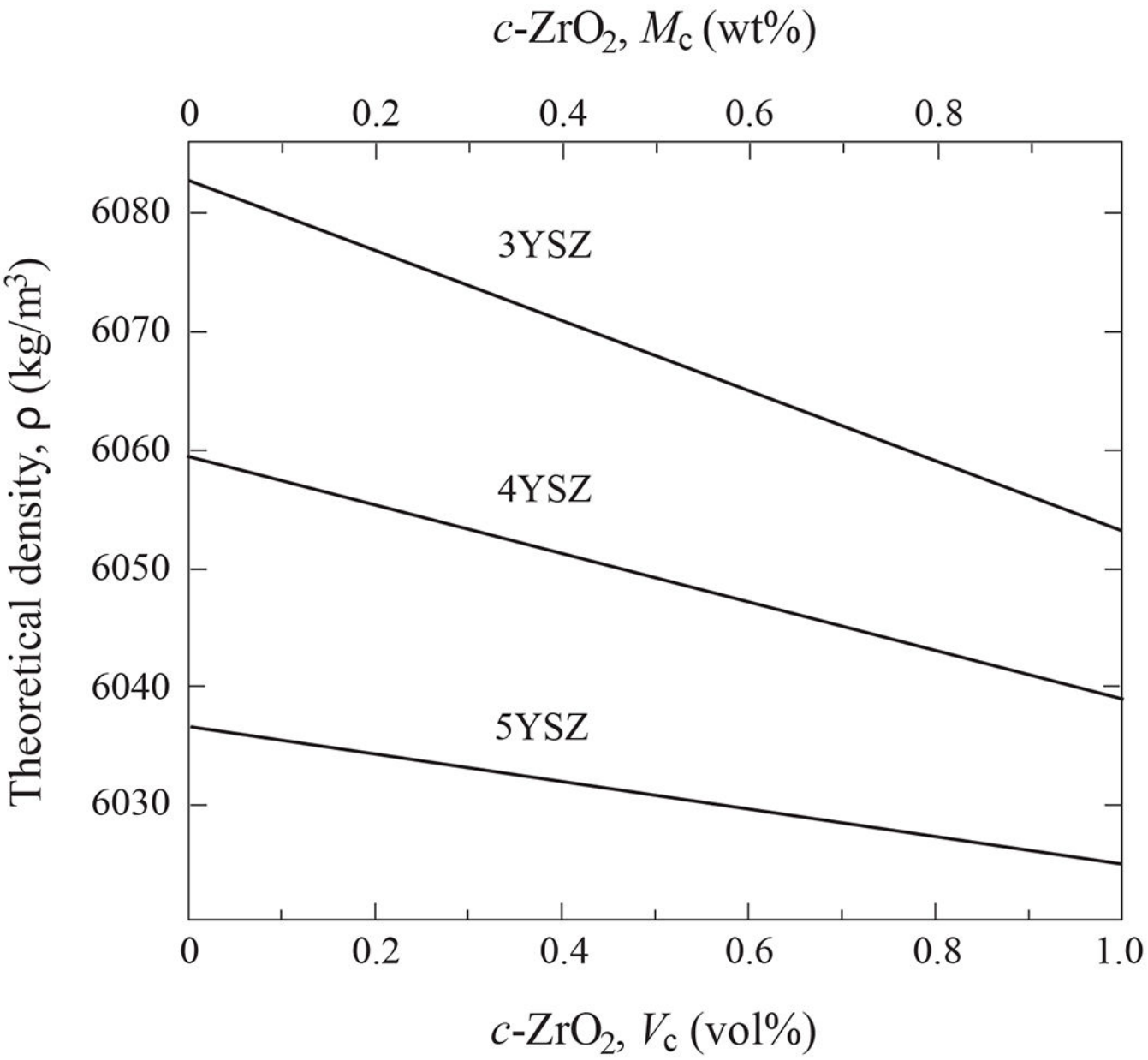

Figure 3.
Theoretical densities of 3YSZ, 4YSZ and 5YSZ ceramics as function of cubic phase mol% (M_c) and vol% (V_c).

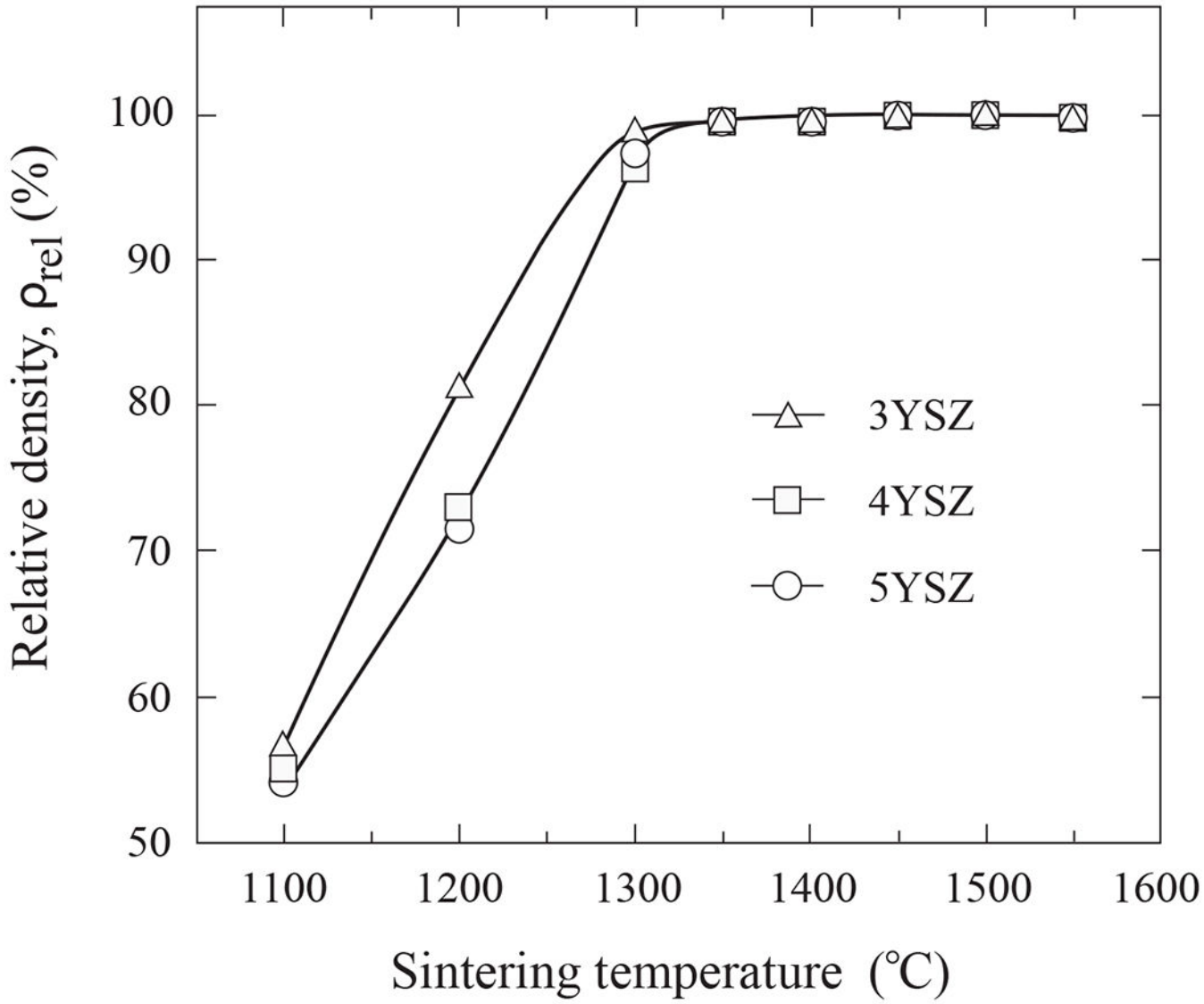

Figure 4.
Relative densities of 3YSZ, 4YSZ and 5YSZ ceramics as function of sintering temperature. Near-full density is achieved over 1350°C.

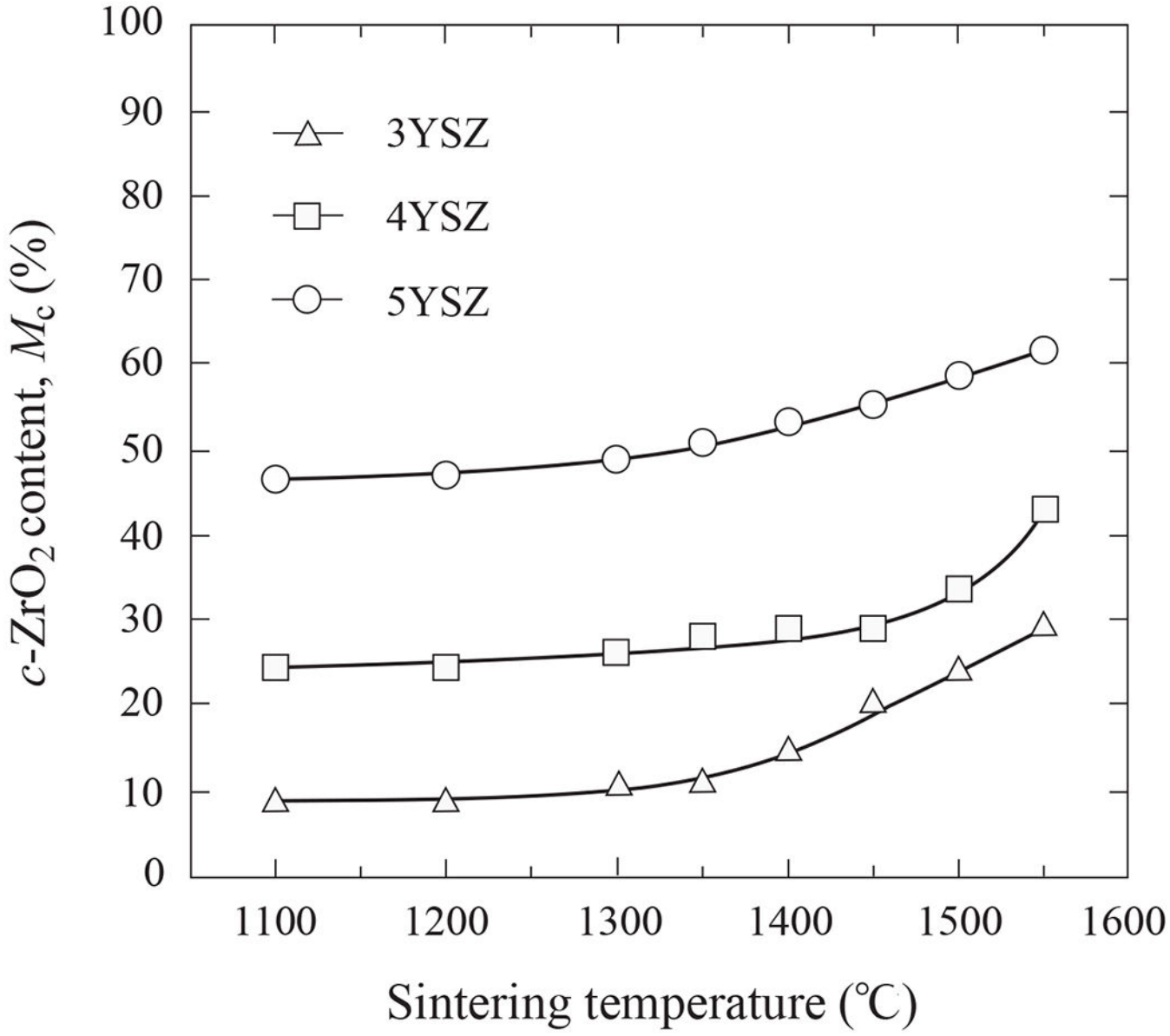

Figure 5.
Cubic phase content of 3YSZ, 4YSZ and 5YSZ ceramics as function of sintering temperature.

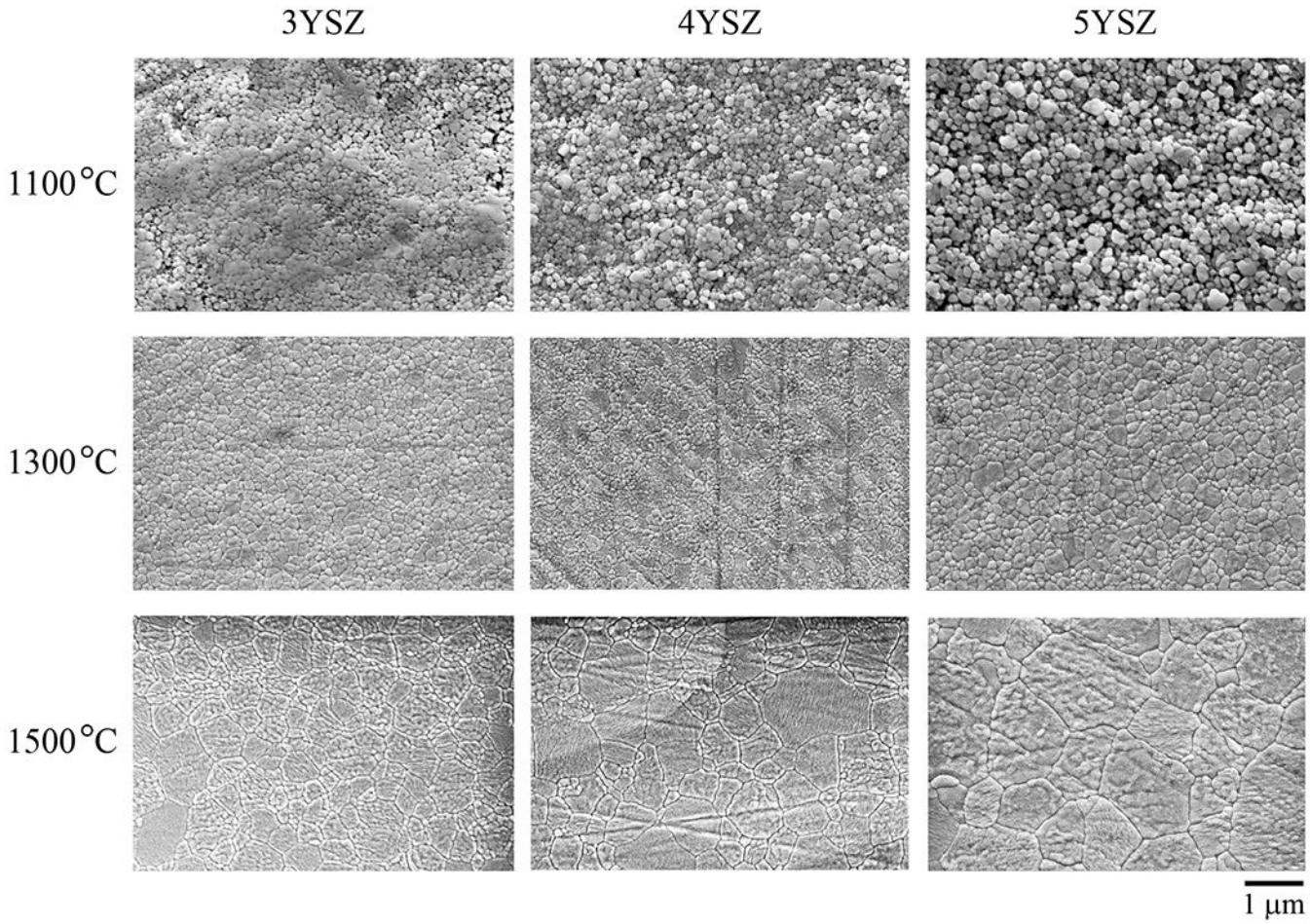

Figure 6.
SEM images of 3YSZ, 4YSZ and 5YSZ for three sintering temperatures. Note consolidation of starting powders and grain growth over the temperature range.

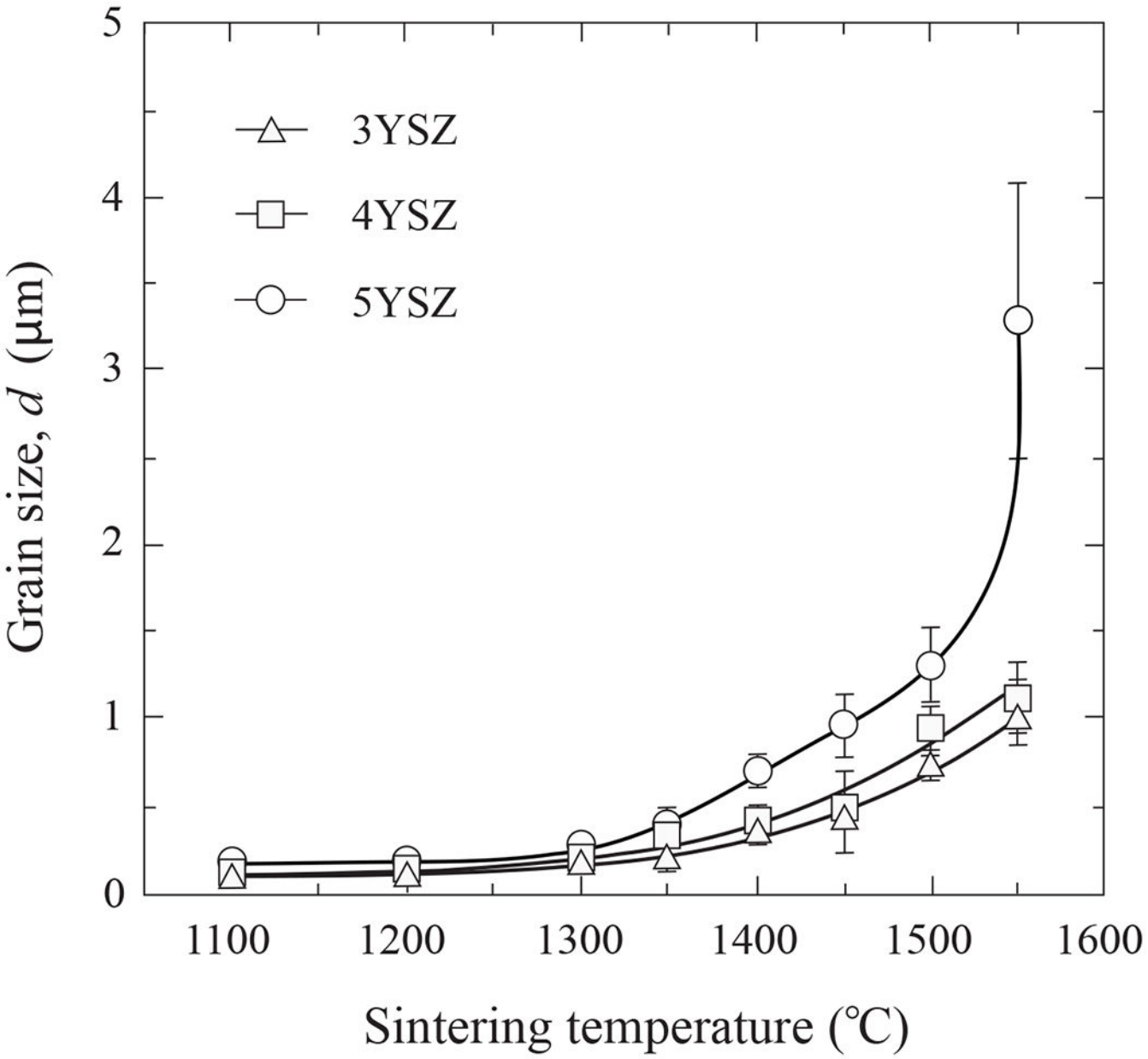

Figure 7.
Grain sizes of 3YSZ, 4YSZ and 5YSZ as function of sintering temperature. Error bars represent one standard deviation of the mean.

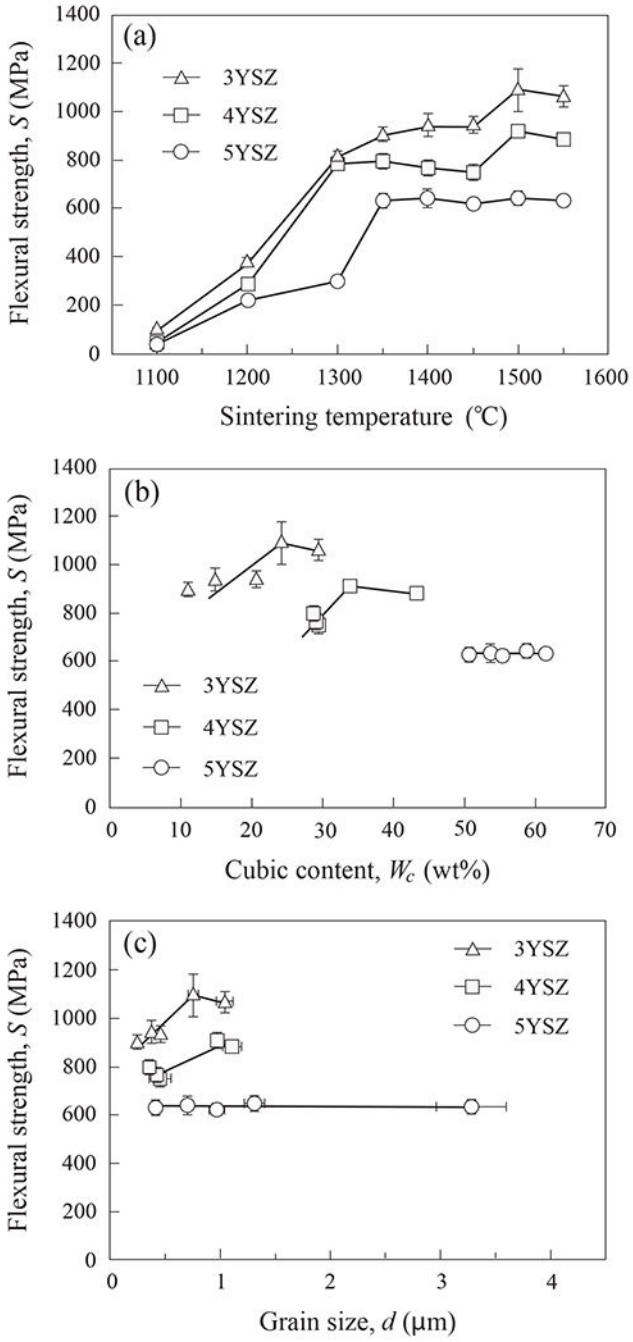

Figure 8.

Strengths of 3YSZ, 4YSZ and 5YSZ as function of (a) sintering temperature, (b) cubic phase content, and (c) grain size. Error bars represent one standard deviation of the mean.

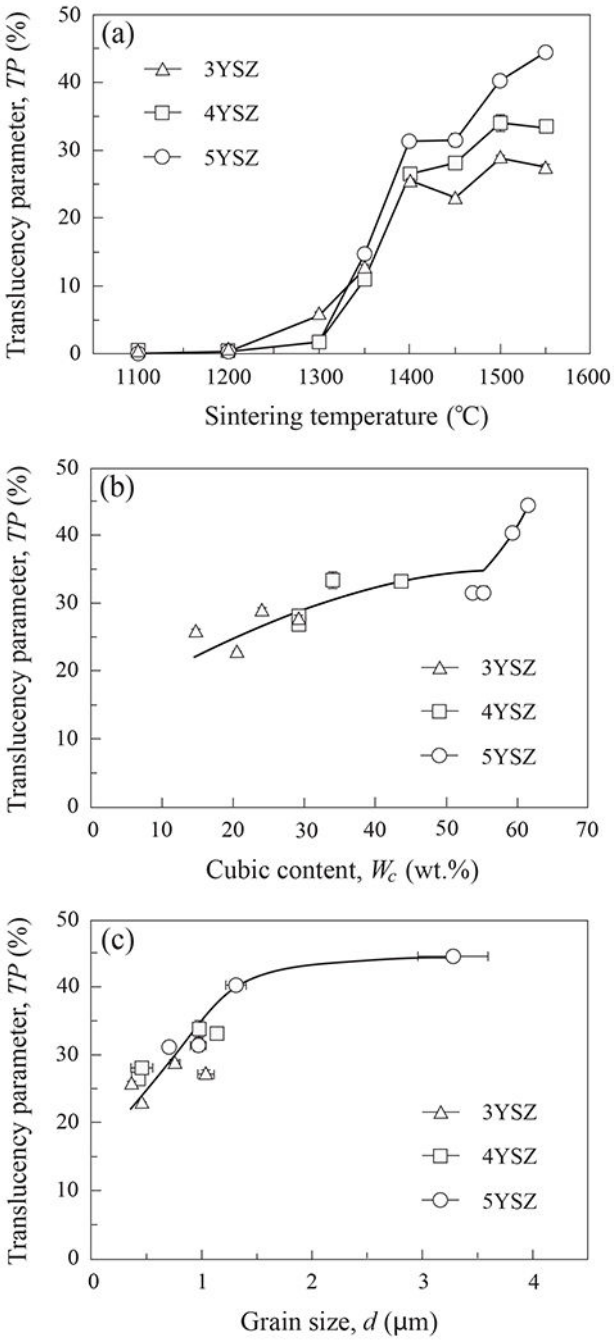

Figure 9.

Translucency of 3YSZ, 4YSZ and 5YSZ as function of (a) sintering temperature, (b) cubic phase content, and (c) grain size. Error bars represent one standard deviation of the mean.

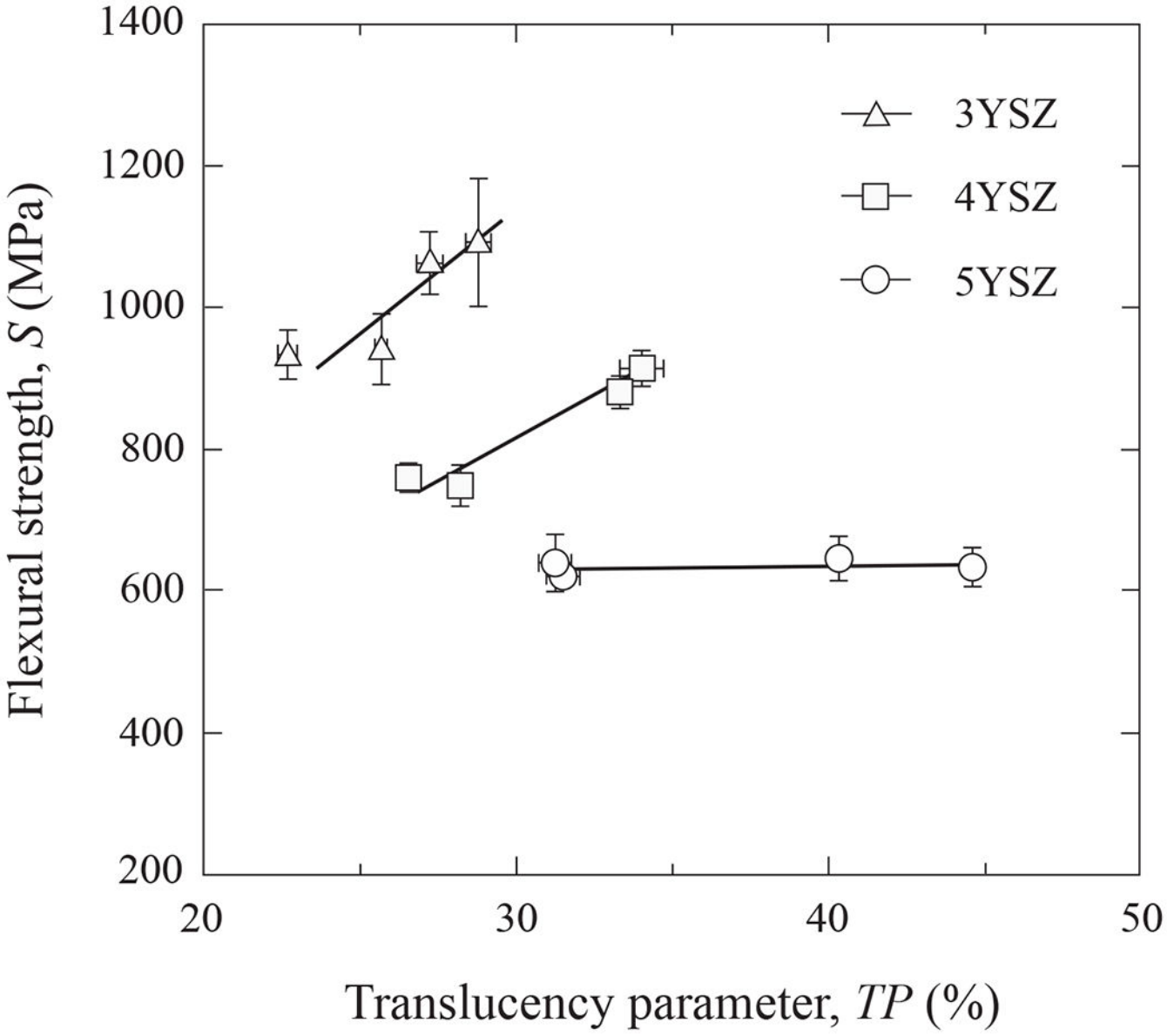

Figure 10.

Flexural strength versus translucency parameter for 3YSZ, 4YSZ and 5YSZ. Note positive correlation for all ceramics except 5YSZ. Error bars represent one standard deviation of the mean ($n = 9$).

Table I.

Calculated relative density for yttria stabilized zirconia (YSZ).

Y_2O_3 content (mol%)	Phase	Density (kg/m^3)
3YSZ	Tetragonal	6083
	Cubic	6053
4YSZ	Tetragonal	6060
	Cubic	6039
5YSZ	Tetragonal	6037
	Cubic	6025